

# Multi Phase Flows

Pascal Aeschi, 16-913-410

Sebastian Lang, 16-946-014

Xeno Meienberg, 15-925-290

*Experimental Methods for Engineers  
 ETH Zürich, D-MAVT, Group 14 - 08.11.2018*

## Abstract

In numerous industrial and scientific applications we encounter and use flows which consist of multiple phases. As these so-called multi-phase phase flows are especially difficult to model because of highly nonlinear behaviour, reliable experimental methods and measurements are crucial in order to ensure safety and improve understanding. In this experiment we consider a constant water- and varying air flow through a square channel. With a wire-mesh sensor we conduct four measurements at different volumetric air flow rates, demonstrating various types of bubbly flow. By utilising the different conducting properties of water and air, we are able to determine just how much of each phase is passing through the measuring points of the sensor at any given time. We average this data over the whole measuring duration and plot the respective void fraction distributions of the receiving and the transmitting wires. Through a second layer in the sensor we are able to deduce the velocity of air bubbles by looking at the change in void fraction distributions. A graphical comparison is then made between the measured and the theoretical superficial velocities. The results we get confirm our theoretical hypothesis that smaller bubbles are drawn to the walls, but larger slug bubbles tend to flow in the middle of the channel.

## 1. Introduction

In many engineering applications, the use of different liquids or gases in order to convert or transfer energy are of very high interest. In numerous systems, it occurs quite often that these working fluids cannot be identified entirely as single-phase fluids. They rather appear to be two-phase flows or even multi-phase flows. The distinction between numerous flow regimes in liquid-gas flows is derived by the optical dissimilarities of the gaseous phases, as seen in Fig. 1. In our experiments, we will focus on the bubbly flow regime in Fig. 1a and the slug flow regime, illustrated in Fig. 1b.

For the bubbly flow regime, the liquid flow rate is sufficiently high in order to break the gases into small bubbles. These bubbles are spheri-

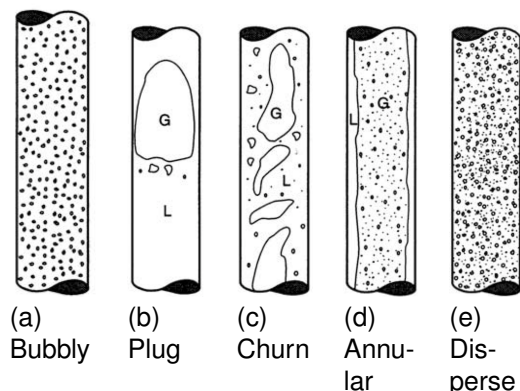


Figure 1: Sketches of different flow regimes in vertical pipes, characterized by the shape of the gaseous components, by Weismann (1983) [Nuclear Power for Everybody (2018)]

## Nomenclature

$\Delta k$ [ ] Time Shift	$J$ [ $\frac{m}{s}$ ] Superficial Velocity
$\varepsilon$ [ ] Void Fraction	$L$ [m] Length
$A$ [ $m^2$ ] Area	$u$ [S] Conductance
$F$ [ ] Cross Correlation Function	$v$ [ $\frac{m}{s}$ ] Velocity

cally shaped and are, in comparison to the tube, marginally large in size.

The slug flow regime appears as soon as numerous bubbles start accumulating, an effect which is induced by higher void fractions. Slugs tend to have a similar diameter as the tube.

It follows that working fluids in condensers and evaporators, chemical reactors or pneumatic actuation cannot always be modeled as fluids with unique thermochemical nor fluid-mechanical properties. For steam-liquid water flows, each volume or mass fractions of each phase show different velocities and temperatures which inhibit different densities [Nuclear Power for Everybody (2018)].

If one wants to observe the highest concentration of bubbles, then different cases have to be accounted for. Small, round bubbles are forced to the walls due to centripetal forces, as they are undergoing a circular motion. If they start to become larger or irregular, they experience a force to the centre of the tube. This is because there the velocity field is the highest, since it rises from the walls to the centre of the tube. [Shew et al. (2006)]

Another problem to account with is the unpredictability of the true nature of multi-phase flows since their behaviour is deemed to be strongly nonlinear. Measurements made by Hewitt and Roberts (1969) [Brennen (2005)] as illustrated in Fig. 2 show the nonlinear relations for liquid-phase and gas-phase momentum fluxes in vertical pipes. For every single regime the resulting fluxes - the flows of both components - do not correspond directly with each other in a fixed rate in order to achieve a certain flow regime.

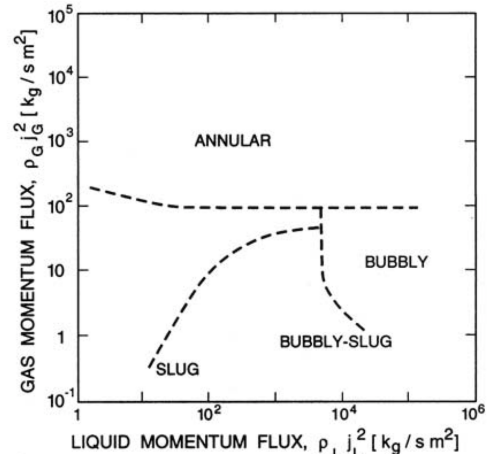


Figure 2: Vertical flow regime map for flow in a 3.2 cm diameter tube for air/water flow at atmospheric pressure and steam/water flow at high pressure from Hewitt and Roberts (1969) [Brennen (2005)]

With given premise, our main goal in a series of experiments is to extract and understand the behaviour of a gas-liquid vertical flow in tubes by means of electrode-mesh tomography based on the research of H.M. Prasser [Prasser et al. (1998)]. In addition, the assimilation of the experimental approach in the field of engineering ought to be a key for studies or theses in future semesters.

The knowledge about multi-phase flows and the detection of possible risks they might impose on society, e.g. failures in nuclear power plants can help to create a safer world.

## 2. Methodology

### Experimental Setup and Conditions

For the generation of the two-phase flow we have a tall  $50 \times 50 \text{ mm}$  upright square channel filled with water that is pumped at a rate of a constant  $69 \frac{\text{l}}{\text{min}}$ . To create the second flow we inject air from the bottom of the cylinder at variable volume flow ranging from  $0.5 \text{ normed } \frac{\text{l}}{\text{min}}$  to  $25 \text{ normed } \frac{\text{l}}{\text{min}}$ . We want our four measuring points to represent a spectrum of flow regimes between bubbly and slug, multiplying the volumetric flow rate of the air by four at each step. To measure the ratio of both phases as well as the superficial velocity we use wire mesh sensors mounted in the channel [Prasser et al. (1998)], with a receiver layer, a transmitter layer and another receiver layer on top. The relevant parameters of the measurement can be found in Tab. 1 below.

Table 1: System relevant parameters

Sampling Frequency	$10'000 \text{ Hz}$
Measuring Duration	$10 \text{ s}$
Distance betw. Measuring Planes	$1.5 \text{ mm}$
Number of Receivers	32
Number of Transmitters	16
Channel Cross Section	$25 \text{ cm}^2$
Water Flow Rate	$69 \frac{\text{l}}{\text{min}}$

In this experiment we use a so-called wire-mesh sensor, which consists of three planes of 16 wires, each separated by  $1.5 \text{ mm}$ . The middle plane is called the transmitter plane, whose wires are orthogonal to the two outer receiver planes. Each crossing of transmitting and receiving wire is a measuring point. It is of utmost importance that we use AC in this experiment as a direct current would result in electrolysis which introduces measuring errors in the best case or perhaps even destroys the sensor in the worst case. A current applied to the transmitting wires results in an induced current in the receiving wires, but only if there is a conducting medium in between, which is water in this case. We assume the conductance value of air  $u_{\text{gas}}$

to be zero and associate the maximum recorded conductance value  $u_{\text{liquid}}$  with water. This means we can deduce the void fraction  $\varepsilon_{i,j,k}$  of the flow at every measuring point  $i, j$  in each frame  $k$  by relating the measured conductance value  $u_{i,j}$  to  $u_{\text{liquid}}$ .

$$\varepsilon_{i,j,k} = 1 - \underbrace{\frac{u_{i,j,k} - u_{\text{gas},i,j}}{u_{\text{liquid}} - u_{\text{gas},i,j}}}_{u_{\text{gas},i,j} \approx 0} = \frac{u_{\text{liquid},i,j} - u_{i,j,k}}{u_{\text{liquid},i,j}} \quad (1)$$

In order to measure at every crossing, we do not excite the transmitting wires at the same time but successively. Consequently the first transmitting wire produces 16 analog current values in the receiving wires, after which the switch is opened for the next transmitting wire. Figure 3 illustrates given procedure more figuratively.

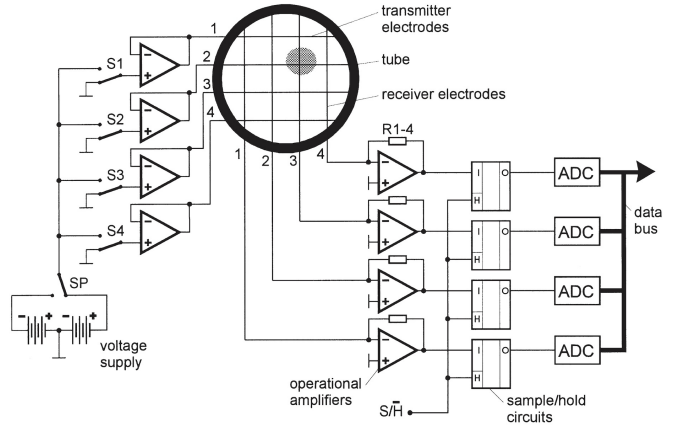


Figure 3: Technical drawing of the mesh [Prasser et al. (1998)]

However, these transmitting wires are only  $3 \text{ mm}$  apart from each other. This means that a significant part of the driving current flows through parallel transmitter electrodes, which are not supplied with voltage from the open switch at the time. These induced currents in transmitting wires result in a current in the receiving wires as well, which blurs the measurements. In order to prevent this cross-talk, the impedance of the transmitter driver output and the receiver input are chosen to be considerably

lower than the impedance of the fluid. Therefore the only non-zero potential of all electrodes belongs to the activated transmitter wire, which is why there is no undesired potential difference for any of the cross-talk currents.

If we only cared about the void fraction, one receiving plane would suffice but as we want to measure the flow velocity distribution as well, we need a second image to compare the two. A bubble traveling through the channel has to pass both sensors, which means we measure the same bubble at two different time frames. We ensure that the bubble passing through the second sensor is the same as in the first sensor by using the cross-correlation function  $F_{i,j,\Delta k}$ .

$$F_{i,j,\Delta k} = \frac{\sum_k \varepsilon'_{1,i,j,k} * \varepsilon'_{2,i,j,k}}{\sqrt{\varepsilon'_{1,i,j,k}} * \sqrt{\varepsilon'_{2,i,j,k}}} \text{ with } \varepsilon'_{i,j,k} = \varepsilon_{i,j,k} - \bar{\varepsilon}_{i,j,k} \quad (2)$$

At the maximum of the CCF we obtain the time shift  $k_{max}$ , which is then utilised to calculate the velocity  $v_{air,i,j}$ .

$$v_{air,i,j} = \frac{\Delta L}{\Delta k_{max,i,j}} * f_{meas} \quad (3)$$

The theoretical superficial velocity  $J$  is then computed through combining the volumetric flow rate  $V$  and the cross-section area  $A$ .

$$J = \frac{V}{A} \quad (4)$$

We estimate the measured superficial gas velocity  $J_{air,meas}$  using the data we gathered from the wire-mesh sensor: the void fraction  $\varepsilon_{i,j}$ , air velocity  $v_{air,i,j}$ , node area  $A_{i,j}$  and channel area  $A_{channel}$ .

$$J_{air,meas} = \frac{1}{A_{channel}} \sum_i \sum_j \varepsilon_{i,j} * v_{air,i,j} * A_{i,j} \quad (5)$$

### 3. Results and Discussion

*Measurements in terms of maximal values of conductivities*

Figures 4 and 5 depict the measured void fractions on the y-axis, depending on the posi-

tion of the wires in the transmitter and receiver layer of the mesh, defined as measuring points on the x-axis. In total, the series of measurements consists of four test cases, listed in Tab. 2. Each test case differs from one another in terms of initial conditions i.e. different flow rates and attained flow regimes. When comparing each different case for either plane, one can immediately observe an overall rise of the void fraction at every point with increasing flow rate. On the other hand, the observation of each test case on its own reveals a growing disparity of the void fraction from the walls towards the center, especially for higher flow rates. In addition, the overall distribution of the void fraction appears to be very symmetric for high flow rates. For low flow rates, the void fraction distribution shows some kind of skewness.

Table 2: Observed flow regimes at different flow rates ranging between 0.5-25 ln/min listed in ascending order

Test Case	Flow Regime	Flow Rate [ln/min]
1	Bubbly Flow	0.5
2	Bubbly Flow w. Interactions	2
3	Dense Bubbly Flow	8
4	Slug Flow	25

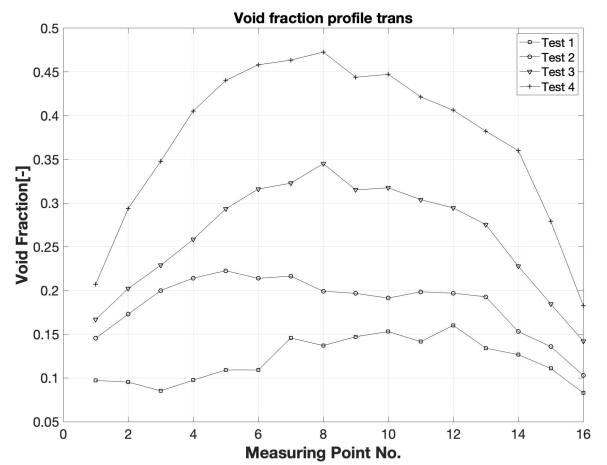


Figure 4: Void fraction profiles of the transmitting wires for each test case

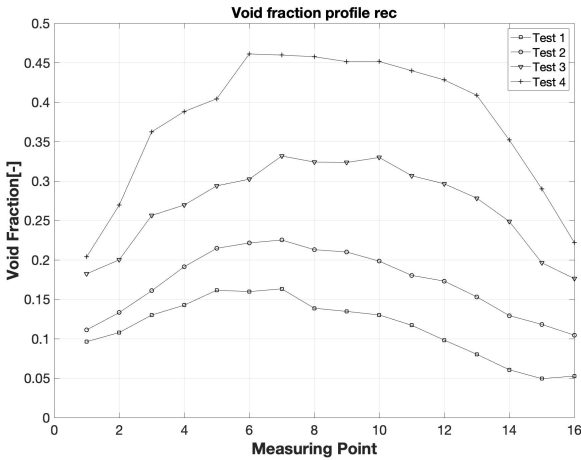


Figure 5: Void fraction profiles of the receiving wires for each test case

Figure 6 is the result from the calculations made in Eq. 5 and the cross- correlation function in Eq. 4 by defining the velocities at each point  $(i, j)$  in the mesh. As explained above, in order to obtain reasonable results, qualifiers were defined to filter noises and disturbances in terms of extremely high or negative velocities and only correlating void fractions below a certain threshold.

By calculating the superficial gas velocity - the average velocity of all gas particles in each cross section - we have a defined base value and the coloured areas depict the relative values in comparison to the superficial velocity.

For our test case one (Fig. 6a) in the bubbly flow regime, it can be observed that levels of equal velocity and closer to the superficial gas velocity than to the zero gas velocity level (coloured in green) were smaller but distinguishable areas of different size. Another fact which can be derived from this plot is the occurrence of exceeding levels in gas velocities (coloured in red).

When we focus on test case two (Fig. 6b) for the bubbly flow with interactions, a substantial change can be seen in terms of the overall distribution of the velocities at each measuring point. The higher velocities (coloured in green) seem to appear near to the center of the cross section and a more continuous and distributed graduation is recognizable although small disparities

are still detectable

In the dense bubbly flow regime in test case three (Fig. 6c), the concentration of higher velocities shifts more to the middle with small disparities in the shape of diamond-like structures. Finally, the distribution has shifted pretty much to the middle of the section.

While observing the plug flow regime in test case 4 (Fig. 6d), the velocities at different points show areas of nearly full superficial velocity. The graduation is more discrete than in test cases two and three while disparities within the measurements have nearly vanished.

Figure 7 shows the measured superficial velocities for all four test cases on the y-axis in comparison to their theoretical superficial velocity on the x-axis. A reference line, the angle bisector, is drawn to visualize parity conditions. Clearly, the case of parity does not hold true since all our obtained data points lie beyond the reference line. In general, the measured superficial velocity is higher than the theoretical superficial velocity, and the deviation from the reference line appears to grow with increasing air flow.

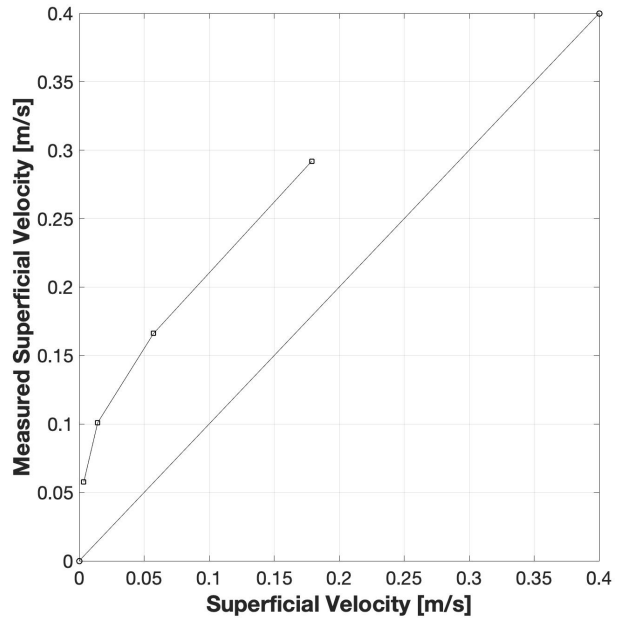


Figure 7: Measurements of the superficial velocity in comparison to the theoretical superficial velocities with parity reference line

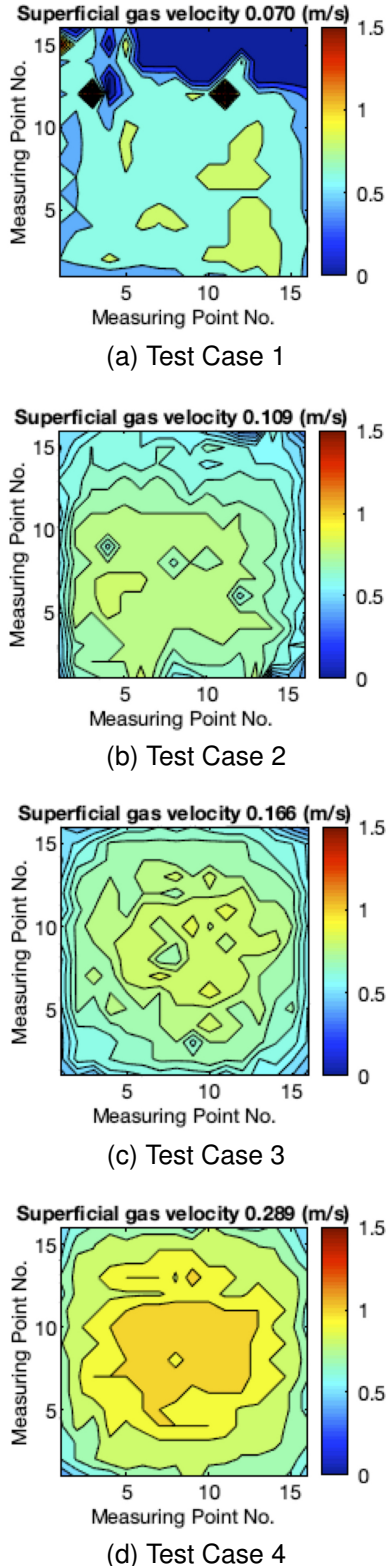


Figure 6: Contour Plot for all four cases at different gas flow rates

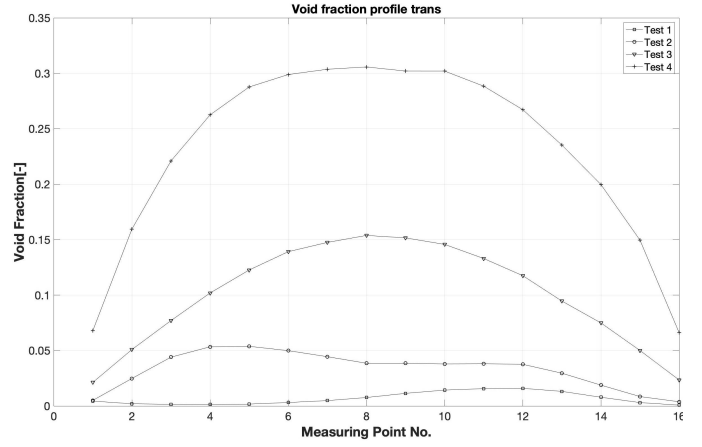


Figure 8: Void fraction profile of the transmitting wires, calculated with respect to saturated water flow

#### *Measurements in comparison to saturated water flow*

In our calculations in Matlab, we previously determined the fractional function by defining the maximal obtained value of each of our matrix entries to be the ideal case of zero gas flow. Although this hypothesis might hold true, another way to reach the zero gas flow condition would be to measure a reference frame i.e. a matrix by switching off the air flow and attaining the conductivity for each measuring point respectively. Figures 8 and 9 depict such a case. Similar to figures 4 and 5, the void fraction profiles on the y-axis depending on the measuring points on the x-axis were then plotted. It can be seen that the properties of the achieved graphs do very much correspond with the preliminary graphs in terms of shape of each test case scenario. The curves appear to be smoother and for higher flow rates in test cases 3 and 4, they look fairly symmetrical with respect to the center of the mesh grid. For test cases 1 and 2, the skewness property is still predominant. In general, the obtained void fractions tend to be much lower than for the previous results.

Figure 10 shows the results from the new calculated velocity, which depend on the void fractions in Fig. 8 and 9 (see above). Here, the same scheme has been used as described from Fig. 6.

Test case one i.e. the observed bubbly flow (Fig. 10a) shows similar features as in test case

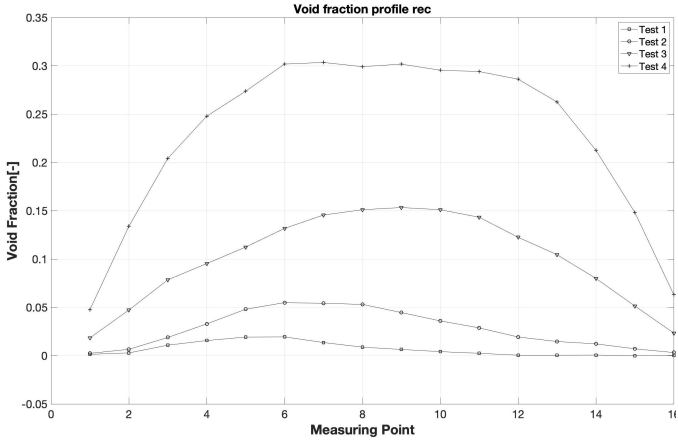


Figure 9: Void fraction profile of the receiving wires, calculated with respect to saturated water flow

one of the measurements depicted in (Fig. 6a), but velocities which outrange the superficial gas velocity were not detectable. As a matter of fact, one larger area enclosing multiple measuring points was found. Smaller areas near to the superficial gas velocity were detected which contain even smaller areas of measuring points, whose values were nearly identical to the measured superficial velocity.

Test case two (Fig. 10b) as well inhibits similar properties as in (Fig. 6b), the centre of the iso-surfaces of the obtained velocities are concentrated to bottom left corner while decreasing from the centre towards the outermost points.

Test case three (Fig. 10c), the equivalent to the observation in (Fig. 6c), demonstrates the tendencies of a centering motion of the velocity field in (Fig. 10b). The drop of each velocity level to another seems to be more continuous, since the boundaries of every surface narrowed to small distances. Again, small irregularities in shapes of smaller quadrilaterals with differing velocities were obtained.

Test case four (Fig. 10d) representing the slug flow regime, the counterpart to the observed test case in (Fig. 6d) contains in comparison to the previous test cases higher relative velocities than in any of the cases in Fig. 10. Towards the middle of the cross section, the velocities of an ensemble of points reach even higher values as the measured superficial gas velocity (coloured in orange). Similar to the the plot

shown in (Fig. 6d), the gradient between each surface of similar velocities tends to be steeper than in the cases from Fig. 10 a,b and c.

Figure 11 shows the resulting, measured superficial gas velocities. Here, the same algorithm was used as for all previous test, again while factoring in the dependency of the newly calculated void fractions illustrated in Fig. 8 and 9. Now, one can observe the nearly perfect parity of the theoretical assumed superficial gas velocity (shown on the y-axis) and the measured gas velocity (shown on the x-axis).

### Discussion

The higher void fraction (especially for lower flow rates) in the lower sensors might stem from the inlet of the gas which is not perfectly centered, but only injected from one side. Otherwise one can observe the expected properties of small bubbles being drawn to the walls, while larger (and irregular) bubbles are drawn to the centre. The superficial velocity is somewhat different but still similar if we do not account for the conductivity of the water flow which we did (as a bonus). We find an almost perfect correlation between superficial velocity and the measured velocity, only at high speeds the measured velocity starts to drop slightly below the superficial velocity. Optimization potential for even more refined measurement would be to improve the grounding of the non active transmitters to prevent noise picked up there. Also the inlet of the gas could be uniform to prevent skewing of the data.

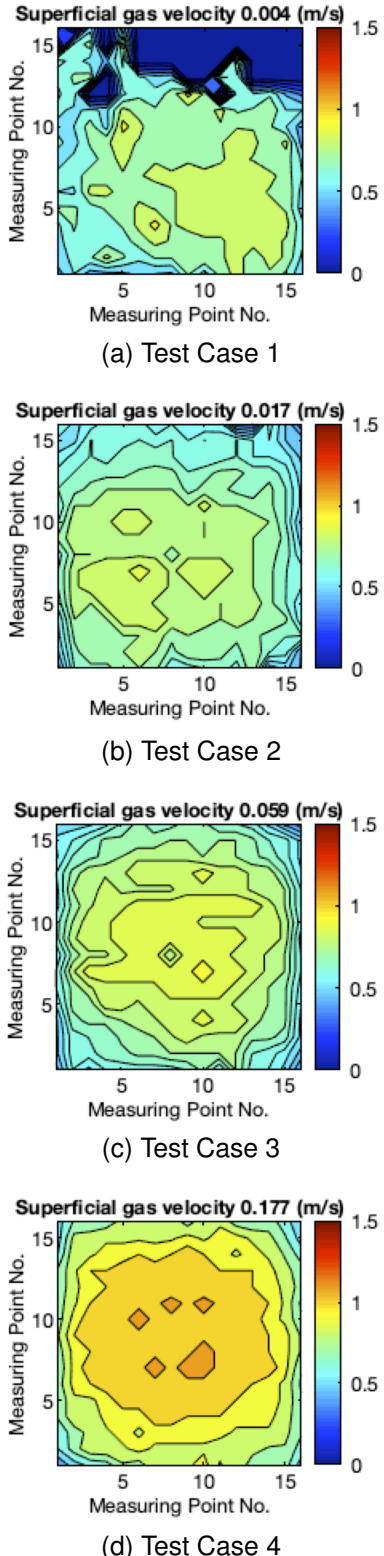


Figure 10: Contour plot for all four test cases, showing measured velocities with respect to the calculated superficial velocity and obtained by the saturated flow data

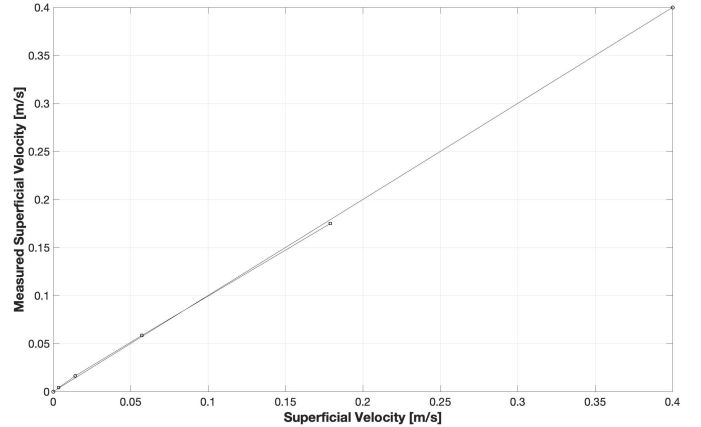


Figure 11: Comparison of the measured velocity and the theoretical superficial velocity of the gas including the parity reference line

#### 4. Conclusions

We measured the void fraction as well as the velocity of four qualitatively different types of flow (0.5, 2, 8, 25 normed  $\frac{l}{min}$ ). For the void fraction we observed that the points with higher concentration agree with the theoretical model, of smaller bubbles being drawn to the sides and larger (and irregular) ones to the centre. For the velocity we found a strong agreement with the superficial velocity after accounting for the water flow saturation, only at high velocities the measured velocity starts to slightly drop below the superficial one. We could observe the different behaviour of two-phase flows and got a first insight into the difficulties and challenges associated with working with them, but as they pose significant effects we have to get a understanding into their workings and how to handle them.

#### 5. References

- Brennen, C. E., 2005. Fundamentals of Multiphase Flows. Cambridge University Press, Cambridge, United Kingdom.
- Nuclear Power for Everybody, 2018. Two-phase flow. <https://www.nuclear-power.net>, [Online; last accessed 20-November-2018].
- Prasser, H.-M., Böttger, A., Zschau, J., 1998. A new electrode-mesh tomograph for gas liquid flows. Flow Measurement and Instrumentation 9, 111–119.
- Shew, W., Poncet, S., Pinton, J.-F., 2006. Force measurements on rising bubbles<hal-00013378v2>.